

EXPERIMENTAL INVESTIGATION OF STATIC INTERNAL PERFORMANCE FOR AN AXISYMMETRIC VECTORING EXHAUST NOZZLE

Jin Jie, Zhao Jingyun, Zhang Mingheng, Lai Chuanxin
Chinese Gas Turbine Establishment

Abstract

An investigation has been conducted in the static nozzle supersonic test facility of Chinese Gas Turbine Establishment to determine the internal performance characteristics of an axisymmetric vectoring thrust nozzle with multiaxis thrust-vectoring capability, which was achieved by deflection of the divergent section of nozzle. The effects of nozzle pressure ratio (NPR) on turning and thrust performance as well as the wall static pressure distributions were studied at varied nozzle geometric vector angle with three different nozzle geometries.

The results of these investigations indicated that while the NPR was less than design pressure ratio, a peak resultant vector angle which was greater than the geometric vector angle occurred and the resultant vector angle was close to the geometric vector angle with the increase of NPR, as well as a peak thrust coefficient occurred near the design pressure ratio and the thrust coefficient slightly decreased with the increase of nozzle geometric vector angle. At lower NPR, the thrust coefficient was high due to flow separation in nozzle. These shown that vectoring of the exhaust flow could be achieved with essentially no addition turning losses within nozzle design pressure ratio compared with existing no-vectoring convergent-divergent exhaust nozzles.

1 Introduction

With the development of the next generation fighter aircraft, some advance performance requirements, such as short take-off and landing, maneuverability at large angles of attack, have been issued and generally accepted. In order to meet these needs, techniques for producing

control forces and moments by redirecting the engine exhaust flow of fighter aircraft have been investigated for several years and different methods and structures of nozzle have been studied to turn the exhaust flow, such as two-dimensional convergent-divergent nozzles (2DCD) with pitch vectoring only [1], spherical convergent flap nozzles(SCFN) with multiaxis vectoring ability [2], pitch/yaw balanced beam nozzles(P/YBBN) [3], axisymmetric convergent-divergent nozzles with post-exit vanes [4] or a gimbaled device [5] and spherical afterburner nozzles with pitch vectoring just applied in Russian Su-37 fighter, and so on. However, large weight or complex structure penalties can occur with the practical use of most nozzles mentioned above. On the other hand, an alternated nozzle design, called axisymmetric vectoring exhaust nozzle (AVEN), which thrust vectoring is achieved by deflection of the divergent section, has been paid the more and more attention in recent years [6]. This design permits divergent flap vectoring through the use of divergent flap active control ring, actuators and by segmented cross joint attachments at the throat. Compared with the other vectoring nozzles, AVEN has following advantages: multiaxis vectoring ability, lighter weight, simple structure and control, etc. But the most benefits is that it can be applied to modify the current axisymmetric convergent-divergent nozzles and promoted the mission performance of fighter without much payment and technical adventure.

The purpose of this investigation is to determine the internal performance characteristics of this AVEN with multiaxis thrust vectoring capability. The fixed-geometry sub-scale nozzle models with different geometry

which simulated the practical engine operation status were tested in the static nozzle supersonic test facility in Chinese Gas Turbine Establishment (CGTE) to determine the turning and thrust performance as well as the internal wall static pressure distribution.

2 Symbols

All the symbols used in the paper including illustrations would be found as follows:

A_e	nozzle exit area, m^2
A_t	nozzle throat area, m^2
P	local wall static pressure, Pa
P_{t0}	jet total pressure of nozzle inlet, Pa
X	axial distance measured from nozzle throat, positive for downstream, m
L	length from the nozzle throat to the exit plane (without vectoring), m
NPR	nozzle pressure ratio
P_0	ambient pressure, Pa
A/B	afterburner
D_e	diameter of nozzle throat, m
F_x	measured axial thrust along body axis (axis X), N
F_y	measured normal thrust (axis Y), N
F_i	ideal isentropic gross thrust, N
F_r	resultant gross thrust, N
Cfr	thrust coefficient
G	measured mass flow rate, Kg/s
R	gas constant for air, 287 J/K m^2
T_{t0}	jet total temperature of nozzle inlet, K
K	ratio of specific heats for air, 1.4
α	convergent angle without vectoring, deg
θ	meridian angle, measured from the bottom of nozzle, positive for counterclockwise, looking upstream, deg
δ	geometric vectoring angle measured from the top or bottom wall without vectoring, deg
δv	resultant vector angle, deg

3 Apparatus and Procedure

3.1 Static Test facility

This investigation was conducted in the static nozzle supersonic test facility in CGTE, which is labeled as SB601. The test apparatus is installed in a room. The jet exhaust to

atmosphere directly through a door aft of the nozzle test apparatus. The control and operation room is just located beside the test room with an observation window made with thick dual-layer optical glass to watch the model and test procedure. This facility uses the clean dry air supply and corresponding air-control system like valves, pipes and filters.

3.2 Propulsion Simulation System

A sketch of air-powered simulation system is presented in fig.1. An external high-pressure air system provided a continuous flow of clean, dry air at a constant stagnation temperature about 310K in nozzles. The air pressure was varied from 1.5 atm to 20 atm ($1 \text{ atm} = 1.013 \times 10^5 \text{ Pa}$). The whole system consists of metric and non-metric parts. The air from the high pressure plenum flows rapidly into the low pressure plenum from opposite directions (perpendicular to the nozzle axis). This method is designed to minimize any forces on the balance imposed by the transfer of axial momentum as the air passed from the non-metric high pressure plenum to the metric low pressure plenum mounted on the force balance. The flexible metal bellows were used as seals between the non-metric and metric portions of the system and served to minimize the axial forces caused by pressurization. The air then flows through a choke plate for flow straightening, through an instrumentation section, and test nozzle which exhausts to atmosphere pressure.

3.3 Nozzle Design and Model

The nozzle design concept permits the multiaxis vectoring of the axisymmetric nozzle through deflection of the divergent section of the nozzle. This is accomplished through the use of a divergent flap active control ring, three actuators and segmented cross joint attachments at the nozzle throat.

The sub-scale models of the axisymmetric nozzle tested during this investigation are shown in fig.2. These nozzles are fixed-geometry representations of a variable-geometry nozzle to simulate the different practical engine

operation status. There are three kinds of nozzles as follows: a) the nozzle expansion ratio was 1.62 and the diameter of throat was 88.3mm, representations of A/B power setting on ground labeled as type A; b) the nozzle expansion ratio was 1.62 and the diameter of throat was 77.1mm, representations of dry power setting on ground labeled as type B; c) the nozzle expansion ratio was 1.20 and the diameter of throat was 77.1mm, representations of cruises power setting in air labeled as type C. The geometric vectoring angle of 5° , 10° , 15° and 20° were provided for each nozzles. The radius of all model nozzles throat is constant as 3mm.

The geometry vectoring angle is measured at the nozzle top or bottom wall from no-vectoring position. This is a little different from the general research. In the practical engine/aircraft operation status, the only geometry controlled by the pilot is the displacement of the three actuators and consequently the rotation angle of control ring as well as the deflection of the flap. Actually the geometry vectoring angle is totally determined and controlled by the deflection angle of the flap. So in this investigation, the deflection angle of the top or bottom wall in divergent section (representation of top or bottom divergent flap in practical nozzle) is used to defined as geometry vectoring angle (δ) and the real local divergent angle of divergent wall is $\alpha + \delta$ (top wall, $\theta = 180^{\circ}$) or $\alpha - \delta$ (bottom wall, $\theta = 0^{\circ}$) or α (middle wall, $\theta = 90^{\circ}$) as shown in fig.2.

3.4 Instrumentation

A four-component strain-gauge balance was used to measure forces and moments on the model. Flow conditions in the nozzle were determined from five stagnation pressure probes and one stagnation temperature probe in instrumentation section aft of the choke plate (see fig.1). The nozzle total pressure was determined from the average of these measurements. The mass flow rate of air supplied to the exhaust nozzle was measured by critical flow venturis. There were thirty internal static pressure orifices on the nozzle wall and

divided into three groups which were located around the meridian direction at $\theta = 0^{\circ}$, 90° , 180° respectively. Each group was ten measurements with three measurements along convergent section, one near the throat and six along the divergent section of nozzle.

3.5 Data Reduction

All data were recorded simultaneously, calculated and output automatic by computer. The main parameters used in the discussion of results are δv , Cfr and NPR which are defined respectively as follows:

$$\delta v = \tan^{-1} (F_y/F_x)$$

$$NPR = P_{t0}/P_a$$

$$Cfr = Fr/F_i$$

$$F_i = G \cdot \sqrt{\frac{2KRT_{t0}}{K-1} \left[1 - \left(\frac{1}{NPR} \right)^{\frac{K-1}{K}} \right]}$$

$$Fr = \sqrt{F_x^2 + F_y^2}$$

The vectoring moments has been measured but didn't issued and discuss in this paper.

4 Results and Discussion

4.1 Internal Pressure Distributions

Internal static pressure distributions are presented in fig.3 to fig.7 for the type A nozzle model with vectoring angles of 0° to 20° . These pressure distributions are typical of the flow characteristics of the other nozzles tested.

The nozzles have significantly different flow characteristics than the unvectored nozzles when vectored. As shown in fig.3, not only the quantities but also the distribution of static pressure has been greatly changed from $\theta = 0^{\circ}$ to $\theta = 180^{\circ}$. These also indicated that the internal flowfield of nozzles have varied from unvectoring nozzles and become a "real" 3-D flowfield which can't be estimated with empirical 1-D or 2-D methods any more. It's necessary to investigate and evaluated the flow characteristics and performance of vectoring nozzle. Within the convergent section ($X/L < 0$), the pressure distributions, which has been

influenced by the vectoring of flow in divergent section, gradually varied with different meridian angle. The non-symmetric pressure distribution around the circular could result in the non-uniform force on the adjacent convergent flap and an “extra” moments will occurred between the convergent flap to increase the loading of flap.

The influence of NPR on the pressure distribution around the circular have shown in fig.4~fig.6 with the same resultant vector angle ($\delta = 20^\circ$). At the top wall ($\theta = 180^\circ$), the local geometry expansion angle in divergent section is the largest ($\alpha + \delta$) and within the divergent section ($X/L > 0$), the pressure distribution almost keeps constant and has a little increase without decrease downstream the throat as shown in fig.4. This means that the flow separation has occurred in the top portion accompanying with the inclined shock wave while the nozzle was operated at “over-expansion” status since the NPR is less than the fully expansion pressure ratio which is nearly 7.2 for the nozzles tested. These resulted in the subsonic flow downstream the shock wave and the ambient high pressure air may reverse to “fill” partially the low pressure zone caused by the flow separation at the low NPR.

Fig.5 clearly shows that at the bottom wall ($\theta = 0^\circ$), where the local geometry expansion angle in divergent section is the smallest ($\alpha - \delta$), the pressure distributions are similar to decrease within the all nozzle at different NPR except 1.51, which is less than the critical pressure ratio. These indicate that the flow separation or shock wave or air counterflow is no longer existed near the bottom portion.

The pressure distribution of middle wall ($\theta = 90^\circ$) is nearly coincide with the typical non-vectoring convergent divergent nozzles as shown in fig.6.

The influence of resultant vector angle on the pressure distribution is shown in fig.7. The position of static pressure increase gradually shifted upstream with the increase of resultant vector angle. This means that the flow separation zone will expand when the resultant vector angle is enlarged at the same median position.

4.2 Nozzle Static Performance

The nozzle turning performance studied in this investigation is mainly the influence of NPR on resultant vector angle (δv) as shown in fig.8 and fig.9. For type A model nozzle, δv has a peak value which was greater than geometry vectoring angle and was close to the geometry vectoring angle with the increase of NPR as shown in fig.8. The NPR where the peak resultant vector angle occurred was a little different with geometry vectoring angle but less than the design pressure ratio, which was about 7.2 to the nozzle tested. This effect of thrust angularity varying with NPR occurred where the top portion ($\theta = 180^\circ$) of the divergent flap section extends beyond that of the bottom ($\theta = 0^\circ$), that is to say, the top flap is “longer” than the bottom one relative to the exit plane which is perpendicular to the flow centerline.

Fig.9 shows the influence of operation status on resultant vector angle. The distributions of resultant vector angle with different geometry are almost the same except that the NPR where the peak resultant vector angle occurred varied with the area ratio between exit and throat which the design pressure ratio is determined. On the other hand, the resultant vectoring angle slightly decrease with the increase of throat area as shown in fig.9. That means the turning performance without A/B will be better than that with A/B.

The typical nozzle thrust performance Cfr was studied in the investigation as shown in fig.10 and fig.11. Fig.10 shows that a peak Cfr was occurred near the design pressure ratio just as the turning performance mentioned above. Compared with the unvectored nozzles [6], the peak or maximum obtainable nozzle performance of vectored nozzles was nearly the same as that of unvectored nozzles because the flow was turned essentially at subsonic Mach number in divergent section near the design pressure ratio. At lower NPR, the Cfr was high due to the flow separation in nozzle and counterflow from ambient high pressure air, which result in the increase of the wall static pressure and hence the increase of thrust. This implied that the vectoring of the exhaust flow

could be achieved with essentially no addition turning losses within nozzle design pressure ratio compared with existing no-vectoring convergent-divergent exhaust nozzles.

At high NPR (greater than design pressure ratio), the nozzle operated below fully expansion while the flow separation zone increased without the counterflow from air and resulted in slightly decrease of Cfr with the increase of geometry vectoring angle from 5^0 to 20^0 as shown in fig.10.

Fig.11 indicated the influence of nozzle geometry on Cfr. The thrust performance at lower Ae/At decreased more rapidly than that of higher ones. And the difference of Cfr between the different throat areas(type A and type B) was less than 1%. These implied that the thrust performance at air cruise without A/B may be worse than that of performance with A/B.

5 Conclusion

Based on the discussion of the results obtained from the experimental, the following conclusion could be made:

1. The vectoring nozzles have significantly different flow characteristics compared with unvectoring nozzles and the former empirical 1-D or 2-D methods used to estimate the internal 3-D flowfield would be unavailable any more.
2. While the NPR was less than design pressure ratio, a peak resultant vector angle which was greater than the geometric vector angle occurred and the resultant vector angle was close to the geometric vector angle with the increase of NPR.
3. A peak thrust coefficient occurred near the design pressure ratio and the thrust coefficient slightly decreased with nozzle geometric vector angle varied from 5^0 to 20^0 .
4. The vectoring of the exhaust flow could be achieved with essentially no addition turning losses within nozzle design pressure ratio compared with existing no-vectoring convergent-

divergent exhaust nozzles.

5. The test results could be applied to estimate the performance of practical axisymmetric vectoring thrust nozzles and evaluate the calculation results of nozzle internal 3-D flowfield for the engineering design of axisymmetric vectoring thrust nozzles.

References

- [1] Richard J. Re, Laurence D. Leavitt. *Static internal performance including thrust vectoring and reversing of two-dimensional convergent-divergent nozzles*. NASA TP-2253,1984
- [2] John G. Taylor. *Static Investigation of a two-dimensional convergent-divergent exhaust nozzle with multiaxis thrust-vectoring capability*. NASA TP-2973,1990
- [3] F. Capone, P. Smereczniak, D. Spetnagel, E. Thayer. *Comparative investigation of multiplane thrust vectoring nozzles*. AIAA 92-3263
- [4] Bobby L. Berrier, Mary L. Mason. *Static performance of an axisymmetric nozzle with post-exit vanes for multiaxis thrust vectoring*. NASA TP-2800,1988
- [5] Bobby L. Berrier, John G. Taylor. *Internal performance of two-nozzles utilizing gimbal concepts for thrust vectoring*. NASA TP-2991, 1990
- [6] George T. Carson, Francis J. Capone. *Static internal performance of an axisymmetric nozzle with multiaxis thrust vectoring capability*. NASA TM-4237, 1991

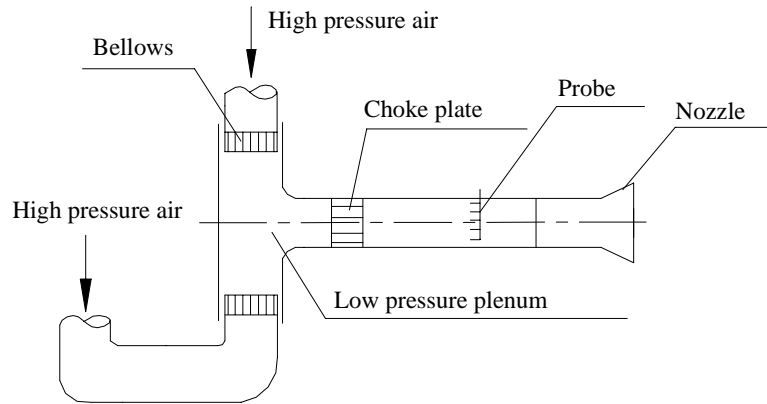


Fig.1 Sketch of propulsion simulation system

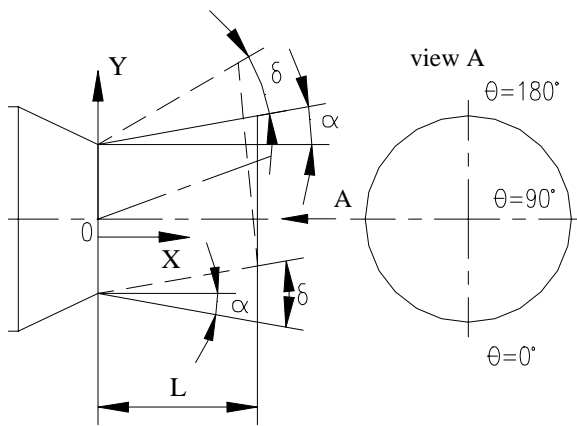


Fig.2 Scheme of AVEN model nozzle

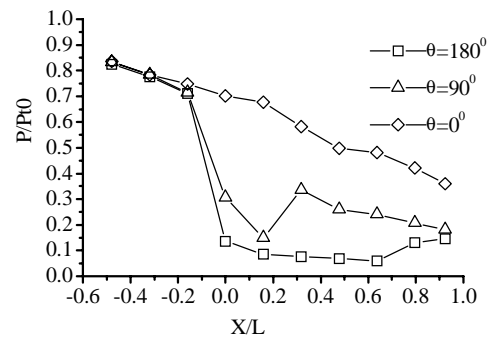


Fig.3 Wall static pressure distributions, Type A, NPR=6.82

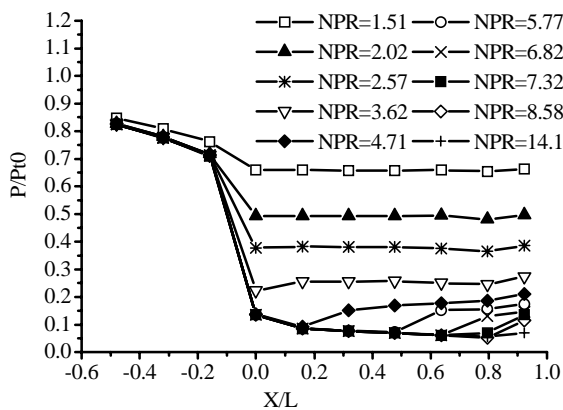


Fig.4 Wall static pressure distributions, Type A, $\theta=180^\circ$, $\delta=20^\circ$

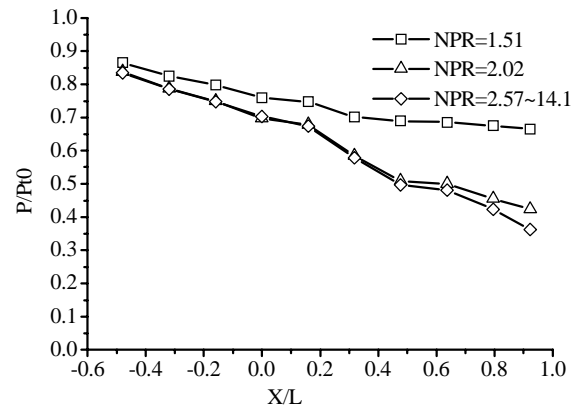


Fig.5 Wall static pressure distributions, Type A, $\delta=20^\circ$, $\theta=0^\circ$

**EXPERIMENTAL INVESTIGATION OF STATIC INTERNAL PERFORMANCE
FOR AN AXISYMMETRIC VECTORING EXHAUST NOZZLE**

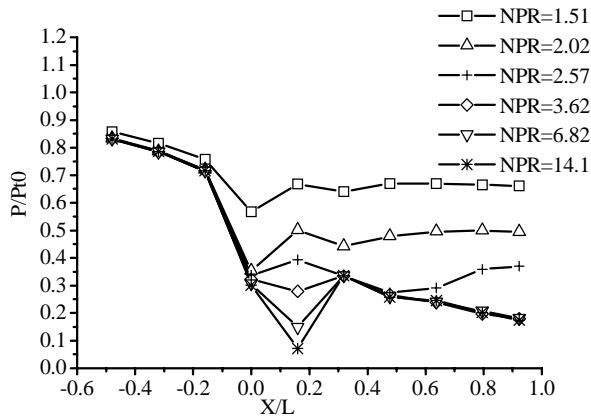


Fig.6 Wall static pressure distributions, Type A, $\delta=20^\circ, \theta=90^\circ$

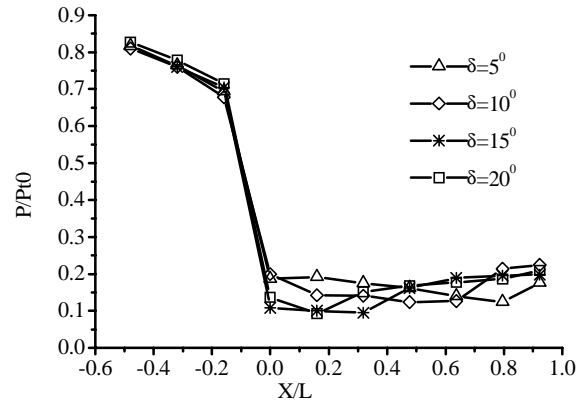


Fig.7 Wall static pressure distributions, Type A, $\theta=180^\circ, NPR=4.7$

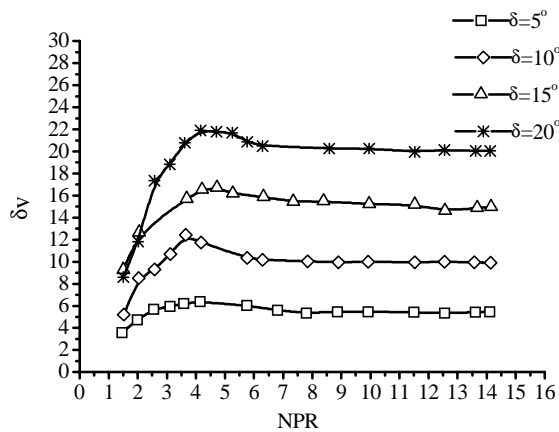


Fig.8 Effect of NPR on turning performance, Type A

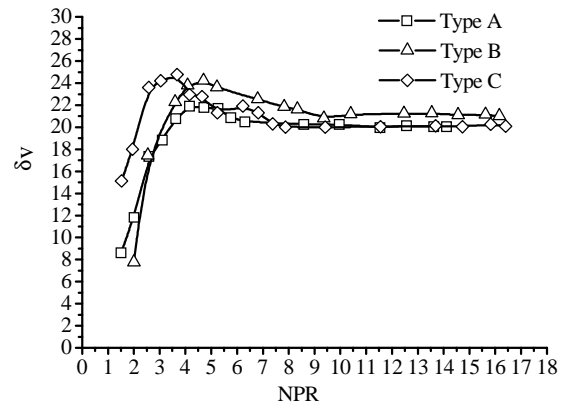


Fig.9 Effect of NPR on turning performance, $\delta=20^\circ$

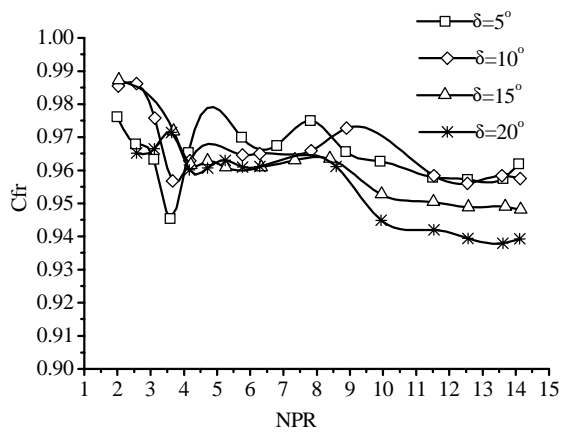


Fig.10 Effect of NPR on thrust performance, Type A

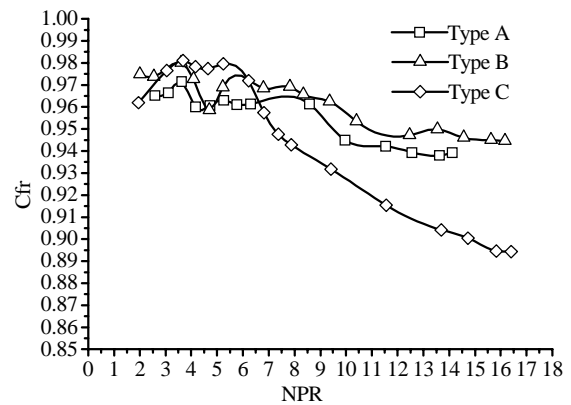


Fig.11 Effect of NPR on thrust performance, $\delta=20^\circ$